Global Change Biology

WILEY

Global Change Biology

RESEARCH ARTICLE

National Evidence of Depth-Dependent Stabilization and Controls of Soil Organic Carbon in Dryland Croplands

Yuchen Wei[1] | Xin Zhao[2] | Wenting Feng[3] | Hongyong Sun[4] | Jinfeng Chang[1] | Hong Chen[1] | Ji Chen[5] | Xiaowei Guo[6,7] | Di He[8] | Feng Liu[9] | Alain F. Plante[10] | Zhou Shi[1] | Zhaoliang Song[11] | Raphael A. Viscarra Rossel[12] | Lewis Walden[12] | Enli Wang[8] | Mingming Wang[1] | Liujun Xiao[13] | Su Ye[1] | Shuai Zhang[1] | Hangxin Zhou[1] | Zhongkui Luo[1]

[1]State Key Laboratory of Soil Pollution Control and Safety, Zhejiang Key Laboratory of Agricultural Remote Sensing and Information Technology, Ministry of Education Key Laboratory of Environment Remediation and Ecological Health, College of Environmental and Resource Sciences, Zhejiang University, Hangzhou, China | [2]College of Agronomy and Biotechnology, China Agricultural University, Key Laboratory of Farming System, Ministry of Agriculture and Rural Affairs of the People's Republic of China, Beijing, China | [3]School of Grassland Science, Beijing Forestry University, Beijing, China | [4]Key Laboratory of Agricultural Water Resources, Center for Agricultural Resources Research, Institute of Genetics and Developmental Biology, Chinese Academy of Sciences, Shijiazhuang, China | [5]State Key Laboratory of Loess and Quaternary Geology, Institute of Earth Environment, Chinese Academy of Sciences, Xi'an, China | [6]College of Natural Resources and Environment, Northwest A&F University, Yangling, China | [7]Key Laboratory of Plant Nutrition and the Agri-Environment in Northwest China, MOA, Yangling, China | [8]CSIRO Agriculture and Food, Black Mountain, Australian Capital Territory, Australia | [9]State Key Laboratory of Soil and Sustainable Agriculture, Institute of Soil Science, Chinese Academy of Sciences, Nanjing, China | [10]Department of Earth & Environmental Science, University of Pennsylvania, Philadelphia, Pennsylvania, USA | [11]Tianjin Key Laboratory of Earth Critical Zone Science and Sustainable Development in Bohai Rim, Institute of Surface-Earth System Science, School of Earth System Science, Tianjin University, Tianjin, China | [12]Soil & Landscape Science, School of Molecular and Life Sciences, Curtin University, Perth, WA, Australia | [13]National Engineering and Technology Center for Information Agriculture, Engineering Research Center for Smart Agriculture, Ministry of Education, Key Laboratory for Crop System Analysis and Decision Making, Ministry of Agriculture and Rural Affairs, Jiangsu Key Laboratory for Information Agriculture, Jiangsu Collaborative Innovation Center for Modern Crop Production, Nanjing Agricultural University, Nanjing, Jiangsu, China

Correspondence: Zhongkui Luo (luozk@zju.edu.cn)

Received: 9 May 2026 | **Revised:** 13 July 2026 | **Accepted:** 31 July 2026

Keywords: agricultural management | carbon sequestration | deep soil | mineral-associated fraction | soil organic carbon

ABSTRACT

Soil organic carbon (SOC) underpins agricultural sustainability and the terrestrial carbon cycle, yet its vertical distribution and stabilization across soil depth remain poorly constrained at large spatial scales. Here, we present a nationwide, depth-resolved dataset of SOC and mineral-associated organic carbon (MAOC)—the more persistent SOC fraction—from 365 dryland cropland sites across China, sampled to 2 m depth. Contrary to the classic model of exponential SOC decline, 46% of profiles exhibited uniform or increasing SOC and MAOC with depth, highlighting a substantial role of subsoil carbon. MAOC accounted for more than half of total SOC in most layers, but its relative contribution declined below 1 m, challenging the assumption that subsoil carbon is inherently more stable. Clay + silt content was the strongest predictor for SOC, MAOC, and MAOC/SOC across depths, while vegetation productivity, a proxy for carbon inputs, was positively associated with all three. The influence of clay + silt on MAOC accumulation weakened with depth, and the positive interaction between vegetation productivity and clay + silt weakened or diminished from surface soils to deeper layers. These patterns indicate a transition from joint regulation by carbon inputs and mineral surfaces in surface soils toward an increasingly input-limited regime in deeper layers, as inferred from the depth-dependent changes in the relative importance of vegetation productivity and fine particle content. National mapping estimated

Yuchen Wei, Xin Zhao, Wenting Feng and Hongyong Sun contributed equally.

~19.9 Pg SOC stored within the 0–2 m layer in China's dryland croplands, with 75% below 0.3 m and 60% stabilized as MAOC. These results provide a benchmark for depth-explicit SOC accounting and highlight the importance of aligning carbon inputs with soil mineralogy to enhance whole-profile carbon stabilization and climate mitigation.

1 | Introduction

Soil organic carbon (SOC) is a cornerstone of soil health, agricultural productivity, and the global terrestrial carbon cycle. However, intensive agricultural land use has led to widespread SOC depletion, contributing to atmospheric CO_2 accumulation and undermining long-term soil fertility—threatening both climate and food security (Lal 2004; Luo et al. 2010; Sanderman et al. 2017). In response, a range of SOC-enhancing management practices, such as crop rotation, intercropping, residue retention, and no-tillage, have been promoted (Garland et al. 2021; Wang et al. 2025; Weng et al. 2017). Yet, these interventions overwhelmingly target the topsoil (0–0.3 m), leaving the subsoil largely understudied (Button et al. 2022). Given the marked contrasts in physiochemical conditions, root distributions, and microbial processes along the soil profile, subsoil carbon dynamics cannot be reliably inferred from topsoil behaviors (Button et al. 2022). This vertical complexity underscores a critical need for high-resolution, whole-profile datasets to inform depth-explicit carbon sequestration strategies.

Efforts to enhance SOC sequestration are more effective when they target persistent carbon fractions with long residence times, like mineral-associated organic carbon (MAOC; Lavallee et al. 2020). MAOC is often the dominant SOC fraction in arable soils and contributes to improved soil structure, nutrient retention, and water-holding capacity—all essential for sustaining crop production (Six et al. 2002). Despite its importance, the vertical distribution of MAOC across depths remains poorly characterized. This gap limits our understanding of subsoil carbon persistence and impedes the design of management strategies aimed at whole-profile carbon stabilization (Jobbágy and Jackson 2000; Pries et al. 2023).

Furthermore, MAOC formation and stabilization arise from a combination of microbial processing and mineral protection, but the relative importance of these processes changes with depth (Lavallee et al. 2020). In surface soils, where fresh plant inputs and nutrient availability are high, it is well recognized that MAOC is primarily formed through microbial transformation of plant residues into necromass that becomes adsorbed to mineral surfaces or occluded within aggregates (Cotrufo et al. 2019; Lavallee et al. 2020). In contrast, subsoil MAOC formation depends more on the downward transport of dissolved or particulate organic matter and its subsequent stabilization by abundant mineral sorption sites, often under conditions of low microbial biomass and activity, limited energy availability, and nutrient constraints (Luo et al. 2025; Sierra et al. 2024). While these depth-dependent processes are recognized conceptually, they remain poorly quantified in large-scale, intensively managed agricultural systems. In particular, the depth-specific roles and interactions of mineral conditions (e.g., represented by clay + silt content) with other environmental factors (e.g., climate and vegetative dynamics) in controlling MAOC, as well as SOC, remain unresolved. Whole-profile datasets offer a rare opportunity to address these gaps by quantifying SOC and MAOC stocks across diverse soils and climates, and by disentangling the main and interactive effects of environmental conditions and soil mineralogy on carbon stabilization across depths.

To address these gaps, we established a comprehensive national dataset of SOC and MAOC profiles across China's dryland croplands (excluding paddy fields, Figure 1a). Between 2022 and 2023, we sampled soils at 365 sites spanning all nine agro-ecological zones in China (Figure 1a), measuring SOC and MAOC in up to seven depth layers down to 2 m (0–0.1, 0.1–0.2, 0.2–0.3, 0.3–0.5, 0.5–1.0, 1.0–1.5, 1.5–2.0 m). This resulted in 2234 site-depth measurements (Figure 1a). The ratio of MAOC to SOC (MAOC/SOC) was also calculated to indicate the overall stability and persistence of the total SOC pool (Torn et al. 1997). In parallel, we compiled site-level data on agricultural management (via farmer surveys, Table S1), soil properties, time-series remote sensing data, and climate attributes to identify key predictors of SOC and MAOC variability across the region and depth (Table S2). Leveraging this unique dataset, we also developed machine learning models to predict and map SOC and MAOC stocks across three common depth layers (0–0.3, 0.3–1, and 1–2 m), and compared our results with existing national and global carbon datasets. Our study provides the most spatially explicit and vertically resolved SOC and MAOC assessment to date across dryland croplands of China (if not globally), benchmarking national-scale whole-profile carbon stocks and promoting whole-profile soil carbon management.

2 | Materials and Methods

2.1 | Soil Sampling and Farmer Survey

China's dryland cropping areas (excluding paddy rice fields) cover more than 50% of the nation's total croplands and 6.7% of the nation's land surface (Leading Group Office of the State Council for the Third National Land Survey et al. 2023). These regions exhibit a wide range of climatic conditions, with mean annual temperatures (MAT) ranging from −8.4°C to 26.0°C and mean annual precipitation (MAP) ranging from 13 to 2826 mm. Soil sampling was conducted at 365 sites across this expansive region, encompassing diverse climatic conditions, cropping systems, and soil types (Figure 1a). These sites were visually prescreened using Google Earth to ensure that they are croplands. At the sampling sites, MAT ranged from −2.6°C to 25.2°C, while MAP varied from 43 to 2148 mm, effectively capturing the climatic variability of the region.

In 2022 and 2023, a 10 × 10 m quadrat at each site was established in a field (managed by the same farmer), within which three soil cores were randomly excavated to a depth of 2 m ($n = 3$) using a soil core sampler with a diameter of 7 cm. Soil cores were extracted in 0.1 m depth increments. In cases where the full 2 m depth could not be reached for all three replicates, the maximum depth achieved was recorded for each core. The soil

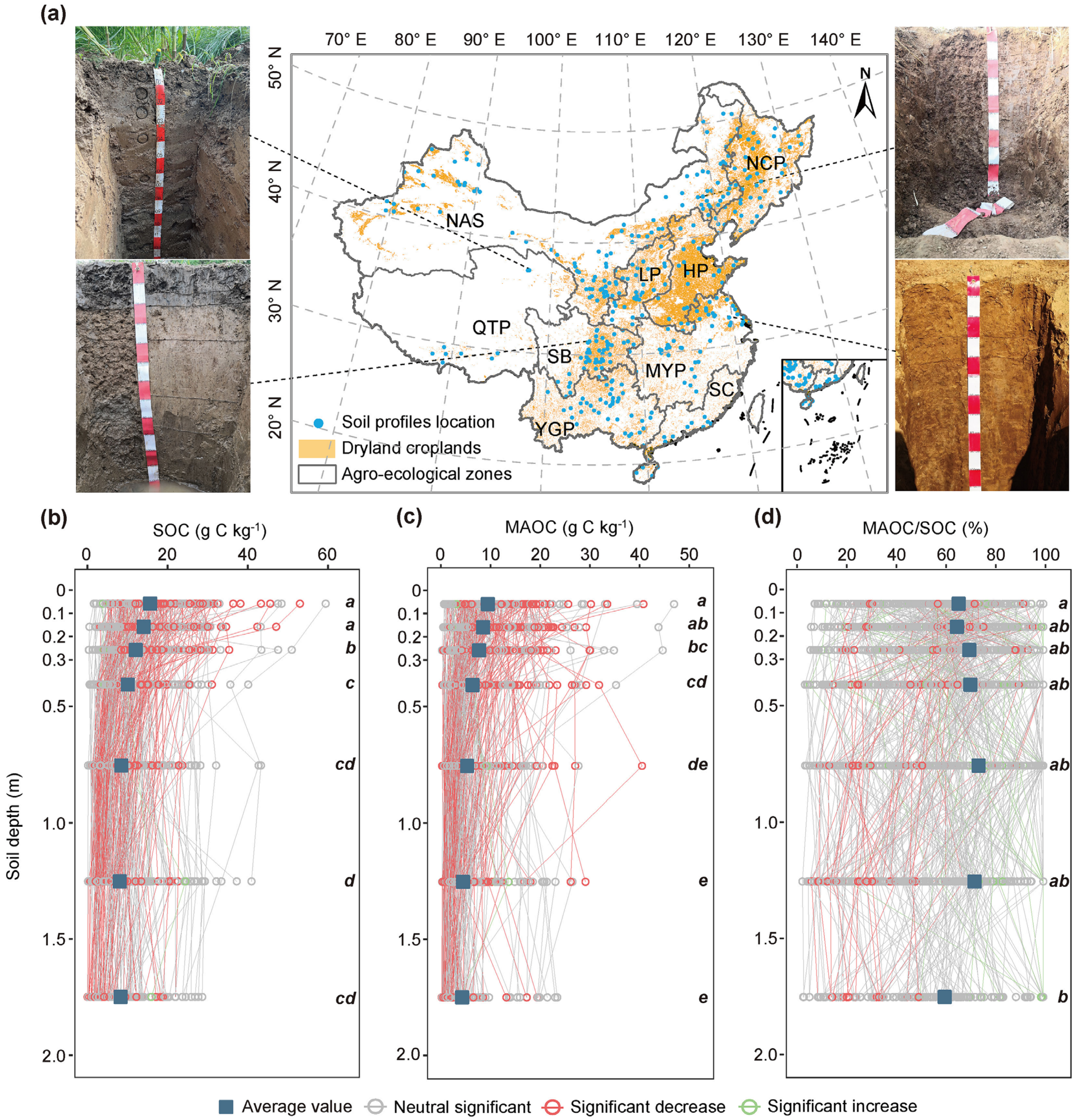

FIGURE 1 | Locations of sampled soil profiles and depth distributions of soil carbon variables. (a) The location of sampled soil profiles and four example profiles. (b-d) Depth distributions of total (SOC, b) and mineral-associated organic carbon (MAOC, c), and their ratio MAOC/SOC (d) across the sampled sites. Squares show the average in each soil depth layer, with different letters indicating significant differences among depth layers at $p < 0.05$. Each line connecting the dots represents one soil profile, with grey, red and green lines representing neutral changes, significant decrease, and significant increase, respectively, identified by fitting linear and exponential regression against depth. Agro-ecological zones are shown as: HP, Huang–Huai–Hai Plain; LP, Loess Plateau; MYP, Middle-lower Yangtze Plain; NAS, Northern arid and Semi-arid region; NCP, Northeast China Plain; QTP, Qinghai–Tibet Plateau; SB, Sichuan Basin and surrounding regions; SC, Southern China; YGP, Yunnan–Guizhou Plateau.

cores were then grouped into seven standardized depth layers: 0–0.1, 0.1–0.2, 0.2–0.3, 0.3–0.5, 0.5–1.0, 1.0–1.5, and 1.5–2.0 m. Samples from the same depth layer within each quadrat were thoroughly mixed and transported to the laboratory for further analysis. At the same time, samples for measuring soil bulk density (BD) were collected at each sampling point to a depth of 0.3 m, divided into three layers (i.e., 0–0.1, 0.1–0.2, and 0.2–0.3 m), with three replicates per layer. Additionally, a representative subset of 20% of sites ($n = 72$) were excavated to a depth of 2 m (Figure 1) to collect samples for measuring BD for the seven standard layers. At the middle of each depth layer, a core ring sampler with a diameter of 5 cm and a volume of 100 cm^3

was used to collect the sample, and brought to the laboratory. We estimated the BD of unsampled deep layers by constructing a random forest (RF) model ($R^2 = 0.77$, root mean square error [RMSE] = 0.12) using the measured BD data and their depths as predictors.

A detailed farmer survey by questionnaire was also conducted by asking the owner farmers of the sampling field to obtain information about management practices (e.g., cropping system, yield, stubble retention, and fertilizer application). The questionnaire is presented in Table S1 with relevant statistics.

2.2 | Measurement of MAOC and Other Soil Properties

The SOC and total nitrogen (TN) contents ($g\,kg^{-1}$) were analyzed in triplicate using an EA 3000 elemental analyzer (Euro Vector, Italy). Specifically, air-dried, 2-mm-sieved soil samples were first acid-treated to remove carbonates prior to SOC analysis. Hydrochloric acid (HCl) was added gradually to the soil samples until visible effervescence ceased, and the samples were then left to react overnight for at least 12 h to ensure complete carbonate removal. The acid-treated samples were subsequently rinsed with deionized water, dried, and sieved through a 0.149 mm mesh to meet the sample preparation requirements for using the elemental analyzer. Soil texture was determined using a laser particle size analyzer (LS-CWM, OMEC, China). Prior to analysis, soil samples were fully dispersed by sequential treatments with HCl and then hydrogen peroxide (H_2O_2) to remove carbonates and organic matter, respectively. Soil BD was determined using the 100 cm^3 soil core ring samples. These samples were dried at 105°C for 48 h, weighed, and corrected for the presence of gravel (> 2 mm).

MAOC was determined by size fractionation following aggregate dispersion, as described in Lugato et al. (2021). Briefly, 5 g of oven-dried, 2-mm sieved soil was treated with HCl to remove carbonates and then agitated with beads for 18 h in a 5 $g\,L^{-1}$ sodium hexametaphosphate solution. Then the dispersed samples were rinsed with deionized water and passed through a 53 μm sieve. The fraction passing through (< 0.053 mm) was collected for measuring SOC which was treated as MAOC. The collected samples were dried at 60°C and analyzed for carbon content in triplicate using the EA 3000 elemental analyzer (Euro Vector, Italy). Because this study focused on the MAOC fraction, which generally represents the more persistent component of SOC, we did not separately quantify the coarse particulate organic carbon (> 53 μm). Accordingly, MAOC content and its proportion of total SOC (MAOC/SOC ratio) were used as indicators of the relative contribution of mineral-associated carbon to the SOC pool, rather than as direct measures of SOC stability (Torn et al. 1997).

The vertical trends of SOC, MAOC, and MAOC/SOC within each soil profile were investigated by fitting both linear and exponential regressions of each variable against depth. The regression coefficients for the depth were then used to classify profiles into three categories: significant increase, significant decrease, and neutral (i.e., no significant change) with depth (Figure 1b–d). A profile was classified as showing a significant increase (or decrease) if either regression yielded a depth coefficient significantly greater (or smaller) than 0 ($p < 0.05$). If both regressions produced coefficients not significantly different from 0, the profile was classified as neutral. The same assessment was applied to the average of each variable across the profiles.

2.3 | Environmental Factors

We collected a set of environmental covariates to explore potential regulators of SOC and MAOC. Table S2 details the covariates and the relevant data sources. Briefly, at each soil profile location, soil clay + silt content was directly measured by this study. For each soil profile, we retrieved the percentage of four mineral types (vermiculite, smectite, kaolinite, and chlorite) from a global dataset of clay-size minerals from Ito and Wagai (2017), mean soil moisture data (i.e., 0.1–1 m depth by 0.1 m intervals) from Li et al. (2022), and soil temperature (i.e., 0–0.2 m depth by 0.05 m intervals) from Wang et al. (2023). At each sampling site, eight topographic predictors (e.g., elevation, slope, aspect) were derived from digital elevation dataset of China (https://data.tpdc.ac.cn/zh-hans/data/12e91073-0181-44bf-8308-c50e5bd9a734), using the System for Automated Geoscientific Analyses Geographic Information System (Conrad et al. 2015; Tang 2019).

Another set of covariates derived from fine-resolution remote sensing images was obtained, including gross primary productivity, vegetation transpiration, soil evaporation, and vaporization of intercepted rainfall products across China during 2000–2020 obtained from Zhang et al. (2019). Additionally, we leveraged Continuous Change Detection and Classification (CCDC) algorithm on all available Landsat 5/7/8/9 Collection 2 surface reflectance data (1984–2024, an average of 1485 images per point) to characterize the temporal dynamics of cropland (Zhu and Woodcock 2014). Normalized Difference Vegetation Index (NDVI) along with seven original Landsat bands were considered. For each 30-m pixel, we applied a harmonic regression on each temporal segment determined by the CCDC algorithm, which decomposed time series of satellite observations into Fourier components including cosine/sine coefficients for the annual cycle (C_1, S_1) and the semi-annual cycle (C_2, S_2; Wilson et al. 2018). Then, we extracted a series of vegetation-related covariates for the temporal segment during which our field visit occurred: (1) NDVI change at the breakpoint (NDVI_ChgMag), which represents the magnitude of vegetation change associated with the most recent natural or anthropogenic intervention; (2) the long-term NDVI slope (NDVI_Trend), reflecting the overall vegetation trend; (3) the amplitude (NDVI_Amp_Annual) of annual cycle, calculated as $\sqrt{C_1^2 + S_1^2}$, representing the intensity of annual vegetation changes; (4) the amplitude (NDVI_Amp_SemiAnnual) of semi-annual cycle, calculated as $\sqrt{C_2^2 + S_2^2}$, measuring the intensity of semi-annual vegetation changes which is often related to double cropping cycles; (5) the mean NDVI to indicate the baseline leaf area index intensity; (6) the goodness-of-fit of CCDC (NDVI_RMSE), which are the residuals from harmonic modeling (i.e., non-seasonal signals) and are often associated with human management; (7) the general disturbance frequency, i.e., the total number of breakpoints detected within the time series (NDVI_Break_count).

Climate variables, represented by the average climatic conditions over the period 1970–2000, were obtained from WorldClim version 2 (Fick and Hijmans 2017; Hijmans et al. 2005). In addition, 33 climate extreme indices (CEIs) defined by the expert team on Climate Change Detection and Indices were extracted from a set of mapping products (at a spatial resolution of 0.25°×0.25°) quantifying the intensity and frequency of climate extremes such as heatwave, cold wave, drought, and heavy precipitation (Alexander 2016). The average CEIs were derived based on sub-daily records of temperature and precipitation at more than 12,000 climate stations across the globe during the period from 1970 to 2016 managed by the Global Land Data Assimilation System (Mistry 2019; Rodell et al. 2004). For all covariate layers, the values at the location of soil profiles were extracted and used in the assessment. Depending on the data format (e.g., grid and polygon) and spatial resolution (e.g., 1 km and 500 m) of covariate layers, different soil profiles in the same grid or polygon share the same value.

Agricultural management variables were obtained directly from farmer questionnaires at each sampling site (Table S1), including fertilizer application rate (kg acre^{-1}), crop yield (kg acre^{-1}), and the proportion of crop residue returned to the field (%), each reported by the owner farmer of the sampled field. Categorical information, such as cropping system and tillage practice, was used to characterize the study system rather than as predictor variables.

2.4 | Predictor Analysis

SOC dynamics are influenced by a variety of factors such as climate, vegetation, edaphic properties, topography, and management practices. To capture potential complex, non-linear interactions between these factors, we applied machine learning-based statistical models, specifically RF, to identify potential environmental predictors for spatial variances in SOC and MAOC contents, as well as the fraction of MAOC in SOC (i.e., MAOC/SOC) across the region and three depth layers. SOC and MAOC concentrations (g C kg^{-1}), originally measured in seven soil layers, were aggregated into three standard depth layers (0–0.3 m, 0.3–1 m, 1–2 m) and an integrated profile (0–2 m). For each standard layer, we fitted a mass-preserving spline function to each soil profile using the *ea_spline()* function in the *ithir* package in R v4.2.2 (Malone et al. 2009; R Core Team 2013). This mass-preserving approach generates a continuous function for the vertical distribution of the soil property throughout the profile, enabling an unbiased estimation of the mean value for any pre-defined depth layer (Luo et al. 2021). Table S2 lists the 78 environmental predictors considered in the analysis. These factors are grouped into six categories: soil properties, terrain attributes, remote sensing variables, agricultural management, climatic variables, and climate extremes. The RF algorithm was implemented with the *train()* function in the *caret* package, using the *ranger* engine (Kuhn 2008; Wright and Ziegler 2017). In brief, RF uses bootstrap sampling to create subsets of the training data via random sampling with replacement, with each subset training an individual decision tree. At each split in a tree, a random subset of features is selected, and the best split is determined from this subset, introducing diversity among trees and reducing overfitting. The model aggregates predictions from all trees by averaging their outputs. To address multicollinearity, we computed variance inflation factors (VIFs) to check for potential collinearity using the *vif()* function in the 'car' package (Fox and Weisberg 2019). Predictors with a VIF of > 5 were excluded from the model. This screening process reduced the set to 37 predictors used in model training. Model performance was evaluated using the determination coefficient (R^2), which quantifies the model's explanatory performance.

The relative importance of each predictor was assessed using permutation variable importance (Breiman 2001). This approach measures the decrease in model accuracy when the values of a predictor are randomly permuted, thereby disrupting its relationship with the target variable. Larger declines in performance indicate greater importance. Importance scores were averaged across permutations and normalized relative to the top predictor (set to 100%) for cross-variable comparison. To further interpret the models, partial dependence analysis was used to quantify the marginal effects of individual predictors on predicted SOC, MAOC, and MAOC/SOC values. This technique isolates the relationship between a given predictor and the model output by varying the predictor across its observed range while holding all others constant (at their mean). The resulting partial dependence plots illustrate non-linear trends and thresholds, offering insight into how specific variables influence soil carbon dynamics.

A primary purpose of this study is to inform management interventions for whole-profile carbon sequestration and stabilization in agricultural soils. Given the critical role of plant inputs in driving soil carbon dynamics and their responsiveness to agricultural management, we synthesized multiple remote sensing vegetation variables (including gross primary productivity [GPP], mean NDVI, NDVI amplitude and change magnitude) to represent plant productivity and its temporal dynamics. Specifically, to reduce dimensionality and integrate these variables into a single indicator, we performed a Principal Component Analysis (PCA) using the base *stats* package in R v4.2.2. The first principal component (PC1), which explained 33.29% of the total variance (Table S3), was extracted and defined as the Vegetation Productivity Index (VPI). VPI is a composite indicator of long-term vegetation productivity and phenology and is interpreted as a proxy for the potential magnitude of plant-derived carbon inputs rather than a direct measure of soil carbon sequestration. We further examined the individual and interactive effects of VPI and clay + silt (c + s), which emerged as dominant controls in the relative importance analysis. Linear mixed-effects models (LMMs) were fitted for SOC, MAOC, and the MAOC/SOC ratio using standardized predictors (z-scores of VPI and c + s), with soil profile (site) included as a random effect factor. These models were implemented using the *lmerTest* package in R v4.2.2, enabling inference on both depth-specific main effects and interactions (Kuznetsova et al. 2017).

2.5 | National Mapping of Soil Carbon Stocks

The fitted RF models were used to predict the spatial distribution of SOC and MAOC stocks across Chinese croplands at a 1 km resolution, for three depth layers: 0–0.3 m, 0.3–1 m, and 1–2 m. Straw return was excluded from the final mapping models due to the lack of spatially explicit data and its low variable

TABLE 1 | Observed depth-specific SOC, MAOC, and the MAOC/SOC ratio across seven depth layers in Chinese croplands.

	SOC (g C kg^{-1})				MAOC (g C kg^{-1})				MAOC/SOC (%)			
Depth (m)	**Mean**	**SD**	**Min.**	**Max.**	**Mean**	**SD**	**Min.**	**Max.**	**Mean**	**SD**	**Min.**	**Max.**
0–0.1	15.7^{a}	9.3	1.6	59.7	9.5^{a}	7.2	0.6	47.6	65.7^{a}	23.7	7.5	98.8
0.1–0.2	14.1^{a}	7.7	0.5	47.3	8.6^{ab}	6.1	0.4	44.4	65.0^{ab}	23.8	6.0	99.2
0.2–0.3	12.1^{b}	7.8	0.3	51.2	7.7^{bc}	6.4	0.2	45.3	70.0^{ab}	24.7	5.8	97.5
0.3–0.5	10.1^{c}	6.4	0.5	40.3	6.4^{cd}	5.8	0.2	35.7	70.5^{ab}	26.0	3.5	97.3
0.5–1.0	8.6^{cd}	7.1	0.2	52.8	5.3^{de}	5.3	0.2	41.0	73.8^{ab}	28.6	3.6	99.7
1.0–1.5	8.1^{d}	7.0	0.1	41.1	4.5^{e}	4.9	0.2	29.5	72.2^{ab}	28.9	2.5	95.2
1.5–2.0	8.3^{cd}	6.7	0.2	28.8	4.3^{e}	5.2	0.1	23.7	60.1^{b}	27.8	2.8	99.6

Note: Different letter superscripts (a–e) indicate significant differences among depth layers at $p < 0.05$.
Abbreviations: MAOC, mineral-associated organic carbon; MAOC/SOC, the percentage fraction of MAOC in total SOC; SOC, soil organic carbon.

importance. Within the remote sensing (CCDC) group, only baseline NDVI and the dominant seasonal predictor NDVI_Amp_SemiAnnual were retained to improve computational efficiency. Model performance was evaluated using fivefold cross-validation, assessed by the coefficient of determination (R^2) and root mean squared error (RMSE; Figure S5). Prediction uncertainty was estimated from the standard error of the 500 individual trees in the RF model (Figure S6).

Spatially explicit predictors were derived from multiple national datasets. Soil texture (c + s) was obtained from a harmonized dataset developed for land surface modeling, based on the 1:1,000,000 scale soil map and 8595 profiles from the second national soil survey (Shangguan et al. 2013). Fertilization rates were sourced from a national dataset of nitrogen fertilizer use spanning 1952–2018 (Yu et al. 2022). Grain yield per hectare was calculated at the county level using 2023 data from Department of Rural Social and Economic Survey of the National Bureau of Statistics of China (2023), by dividing total grain production by sown area. All other spatial predictors were consistent with those described in the "Environmental Predictors" section (Table S2).

SOC and MAOC stocks were aggregated and summarized for China's nine major agro-ecological zones (AEZs) across the three depth layers. These zones reflect differences in climate, land resources, and agricultural systems, and include: Huang–Huai–Hai Plain, Loess Plateau, Qinghai–Tibet Plateau, Middle-lower Yangtze Plain, Sichuan Basin and surrounding regions, Yunnan–Guizhou Plateau, Southern China, Northeast China Plain, and Northern arid and semi-arid region. The AEZ shapefile was obtained from the Data Center for Resources and Environmental Sciences, Chinese Academy of Sciences (http://www.resdc.cn/).

To evaluate the spatial accuracy of our SOC stock estimates, we compared our predictions with three widely used global SOC datasets: the WISE Soil Property Database, the Harmonized World Soil Database (HWSD v1.21), and SoilGrids250m 2.0 (SoilGrids; Batjes 2016; FAO et al. 2012; Poggio et al. 2021). For MAOC, we compared our maps with the global gridded dataset from Georgiou et al. (2022) (Figure S7). All datasets were resampled to a common coordinate reference system, spatial resolution, and extent to ensure comparability.

3 | Results and Discussion

3.1 | Vertical Distributions of SOC and MAOC

On average, SOC content decreased significantly with increasing soil depth (Methods), from 15.7 (range: 1.6–59.7) g C kg^{-1} soil in the 0–0.1 m surface layer to 8.3 (0.1–28.8) g C kg^{-1} in the 1.5–2.0 m layer ($p < 0.001$, Figure 1b, Table 1). However, vertical SOC profiles across China's dryland croplands exhibited striking heterogeneity (Figure S1). At 46% of sites, SOC did not decrease significantly with depth, and two sites even showed increasing SOC with depth (Figure S2a). These deviations from classical exponential decline patterns suggested that vertical SOC dynamics in agricultural soils may be shaped by region-specific processes such as erosion and subsoil deposition, as well as novel agricultural management interventions like deep full-inversion tillage which leads to carbon-rich topsoil burying and incorporation of crop residues to deep layers (Dialynas et al. 2016; Henneron et al. 2022; Jobbágy and Jackson 2000; Liebmann et al. 2020; Luo 2025). In the Loess Plateau—a critical agricultural region in China with very deep soil development, for example, subsoil SOC enrichment was especially prevalent, challenging long-held assumptions about top-concentrated SOC storage in croplands (Wang et al. 2015).

MAOC content displayed depth and spatial distribution patterns similar to those of SOC (Figure 1c). On average, MAOC content decreased from 9.5 (0.6–47.6) g C kg^{-1} at the surface to 4.3 (0.1–23.7) g C kg^{-1} in the deepest sampled layer (1.5–2.0 m). Yet, regional and vertical heterogeneity were again prominent. In 53% of sites, MAOC declined significantly with depth (especially in the Loess Plateau), while 46% showed no apparent depth trend, mainly in arid and semi-arid regions. A small number of sites (1%) exhibited increasing MAOC with depth, pointing to localized processes that favor deep stabilization. On average, surface MAOC content in China's croplands (lumped value of 9.1 g C kg^{-1} in the top 0.2 m) was lower than that in European croplands (13.0 g C kg^{-1}) at comparable depths (Figure 2a), likely

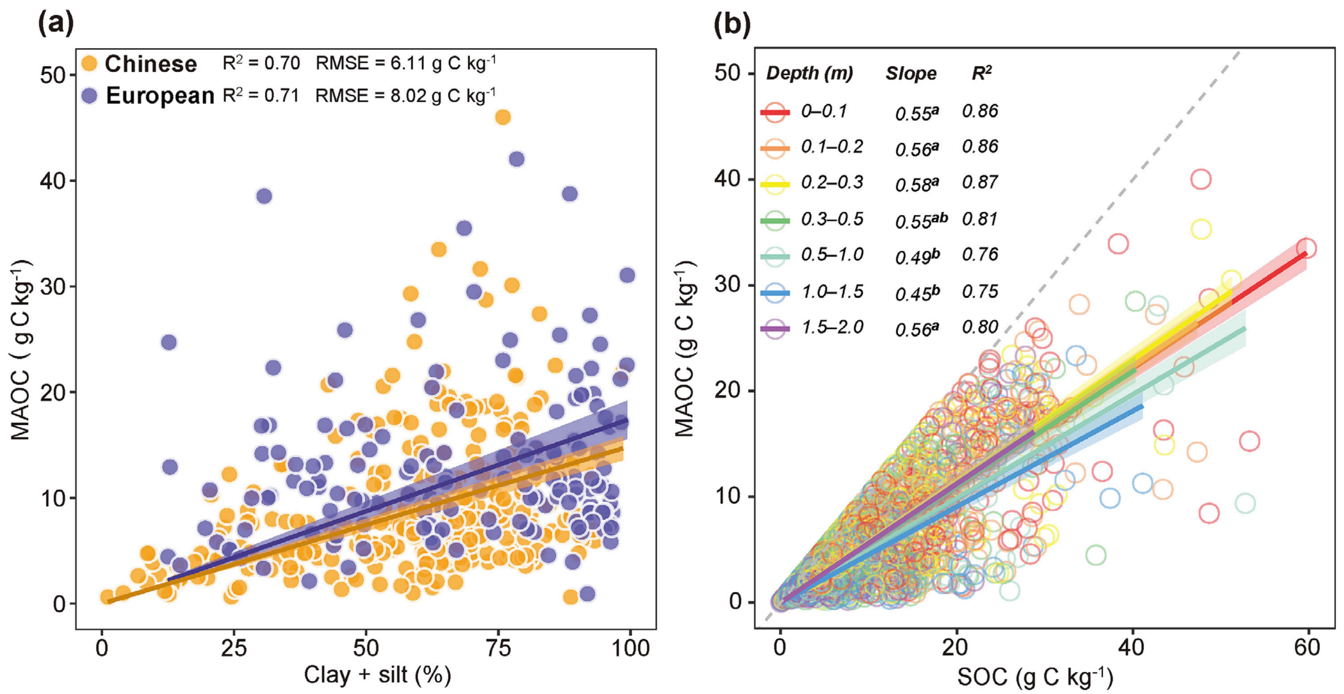

FIGURE 2 | Relationships of mineral-associated organic carbon (MAOC) with clay + silt content and total soil organic carbon (SOC) content. (a) Relationship between MAOC and clay + silt content in Chinese and European croplands. Only data from the 0–0.2 m layer are shown. The data for European MAOC and soil texture are derived from the European LUCAS database (Orgiazzi et al. 2018). (b) Relationship between MAOC and SOC content across seven soil depth layers. Linear regressions without intercepts were fitted for each depth layer. All slopes are significant at $p < 0.001$. Different superscript letters indicate significant differences among depth-specific slopes at $p < 0.05$.

induced by regional contrasts in management history and environmental conditions (Lugato et al. 2021).

MAOC consistently dominated SOC across all depths (i.e., MAOC/SOC > 50%), but its contribution declined with depth—most sharply below 1 m. On average, MAOC accounted for 74% (4%–100%) of SOC in the 0.5–1.0 m layer, decreasing to 60% (3%–100%) in the 1.5–2.0 m layer (Figure 1d). Across all depth layers, MAOC was positively associated with total SOC, without clear signs of saturation (Figure 2b). However, the slope of the MAOC-SOC relationship was steepest in surface soils, suggesting higher efficiency in MAOC formation near the surface, where microbial decomposition is more active and microbial necromass production is enhanced (Sokol and Bradford 2019). Notably, this slope reached a minimum at the 1.0–1.5 m layer. This non-monotonic pattern suggested nonlinear SOC stabilization dynamics across the soil profile. Across the seven individual depth intervals, the relationship between MAOC/SOC ratio and SOC content varied with depth but was generally weak (Figure S3). Significant negative relationships were observed in four layers, particularly in the 0.3–1.5 m layers (Figure S3). However, SOC explained only a small proportion of the variation in the MAOC/SOC ratio ($R^2 \leq 0.04$), indicating that total SOC concentration alone is a poor predictor of the degree of mineral-associated carbon stabilization. These results suggest that increases in SOC do not necessarily correspond to a greater proportion of mineral-protected forms (Liu, Zheng, et al. 2025; Liu, Huang, et al. 2025). The reduced MAOC dominance in deeper layers likely reflects a decline in the processes that form and stabilize MAOC. MAOC forms through two complementary pathways: microbial transformation of organic inputs into microbial products that become stabilized on mineral surfaces, and the direct sorption of plant- and microbial-derived compounds, such as root exudates and extracellular polymeric substances, onto reactive mineral surfaces through adsorption, cation bridging, and association with Fe and Al (hydr)oxides (Cotrufo et al. 2019; Kleber et al. 2015). Both pathways ultimately depend on the availability of fresh carbon substrates, which are generally more limited in deeper layers than near the surface. In addition, intensified environmental constraints on microbial processing, like scarce access to high-quality substrates for energy and nutrient acquisition, as well as diminished oxygen availability, may suppress microbial growth and activity, thereby limiting microbial necromass formation—a key component of MAOC (Bernal et al. 2016; Fontaine et al. 2007; Liang et al. 2019; Rumpel and Kögel-Knabner 2011). Consequently, the lower relative contribution of MAOC at depth is consistent with reduced carbon supply constraining MAOC formation, rather than reflecting suppressed microbial processing alone.

3.2 | Predictors of SOC and MAOC

To disentangle the environmental and management controls on SOC, MAOC, and MAOC/SOC, we aggregated SOC and MAOC data into three depth layers (0–0.3, 0.3–1, and 1–2 m), and an integrated 0–2 m profile (Methods). Random forest (RF) models were employed to quantify the relative importance of a comprehensive set of predictors, categorized into vegetation dynamics, soil properties, topography, climate, and agricultural management (Table S2). These predictors explained over 81% of the variance in SOC, MAOC, and the

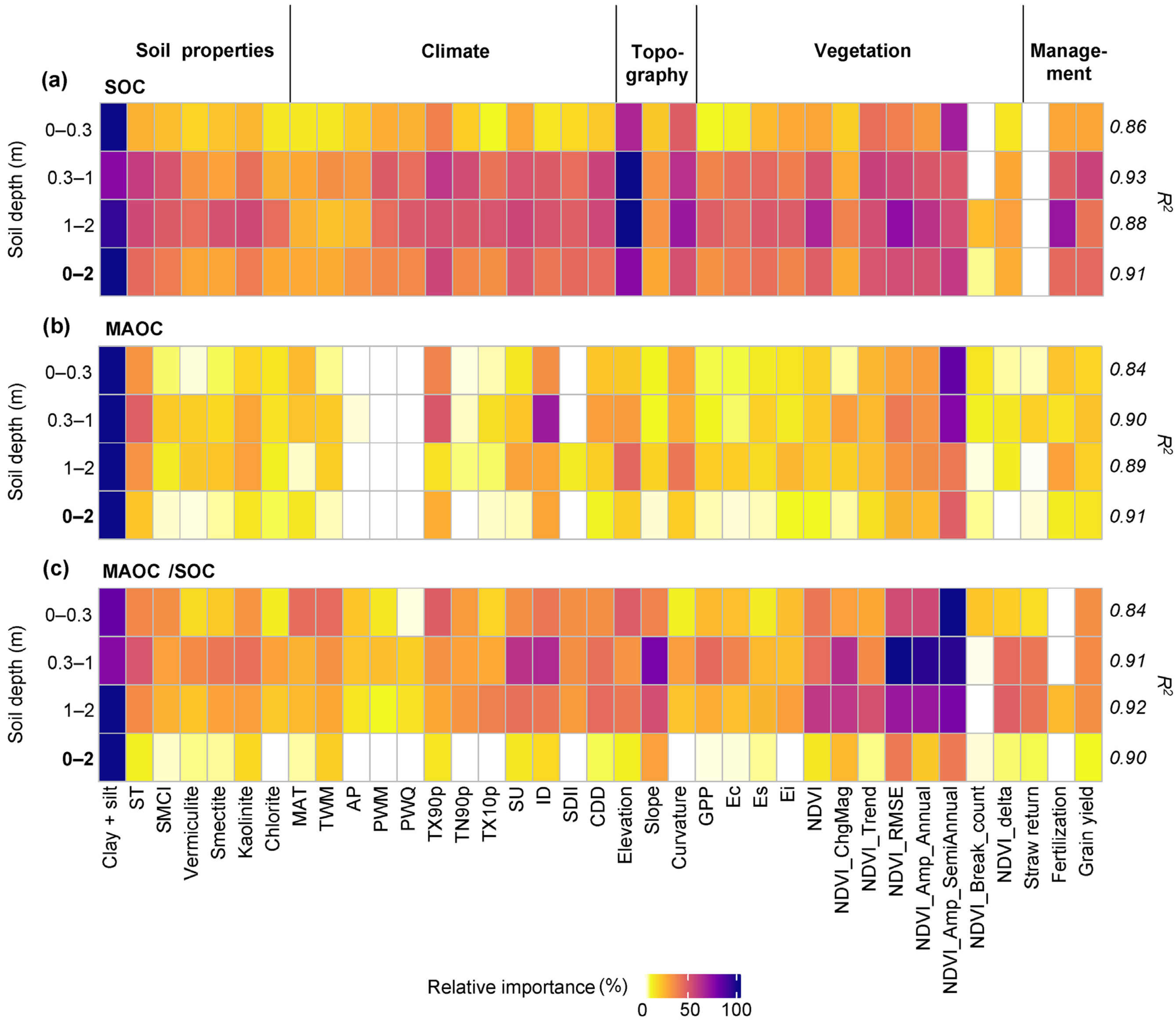

FIGURE 3 | Environmental predictors of soil carbon variables. (a–c) The relative importance of individual predictors for depth-specific total soil organic carbon (SOC, a), mineral-associated organic carbon (MAOC, b), and their ratio MAOC/SOC (c) derived from random forest modeling. The percentage relative importance was normalized to 100% (the most important). Numbers on the right show the determination coefficients (R^2) of the model for the corresponding layer. The most important predictors with high relative importance across depth intervals include: ID, Number of icing days; NDVI_Amp_Annual, Amplitude of the annual (12-month) harmonic component in the NDVI time series; NDVI_Amp_SemiAnnual, Amplitude of the semi-annual (6-month) harmonic component in the NDVI time series; NDVI_RMSE, Root mean square error of the continuous change detection and classification method (CCDC) model fit to the NDVI time series; SU, Number of summer days. A full description of the abbreviations of the predictors is given in Table S2.

MAOC/SOC ratio across the three depth layers (Figure 3), underscoring the strong influence of interacting environmental and management factors on carbon dynamics in intensively managed dryland systems.

Across all depths and carbon fractions, the c + s was the most influential predictor (Figure 3). Partial dependence analyses revealed positive associations between c + s and all three carbon variables (Figure S4), consistent with the role of fine-textured soils in promoting physical protection through aggregation and chemical stabilization via organo-mineral interactions (Georgiou et al. 2022; Kleber et al. 2015; Schweizer et al. 2021). In addition to c + s, remote sensing-derived temporal dynamics of NDVI accounted for a substantial proportion of the explained variance (Figure 4a–c). Temporal variation in NDVI captured seasonal crop phenology and productivity, reflecting both crop-derived carbon inputs and agricultural disturbance (Zhou et al. 2024). In particular, the semi-annual amplitude of NDVI—characteristic of multi-cropping systems such as winter wheat-summer maize rotations, a prevalent system in Chinese dryland croplands—emerged as the most influential vegetation predictor (Liu et al. 2018). Its stronger association with MAOC and MAOC/SOC ratio suggested that intensified cropping may enhance carbon inputs, microbial

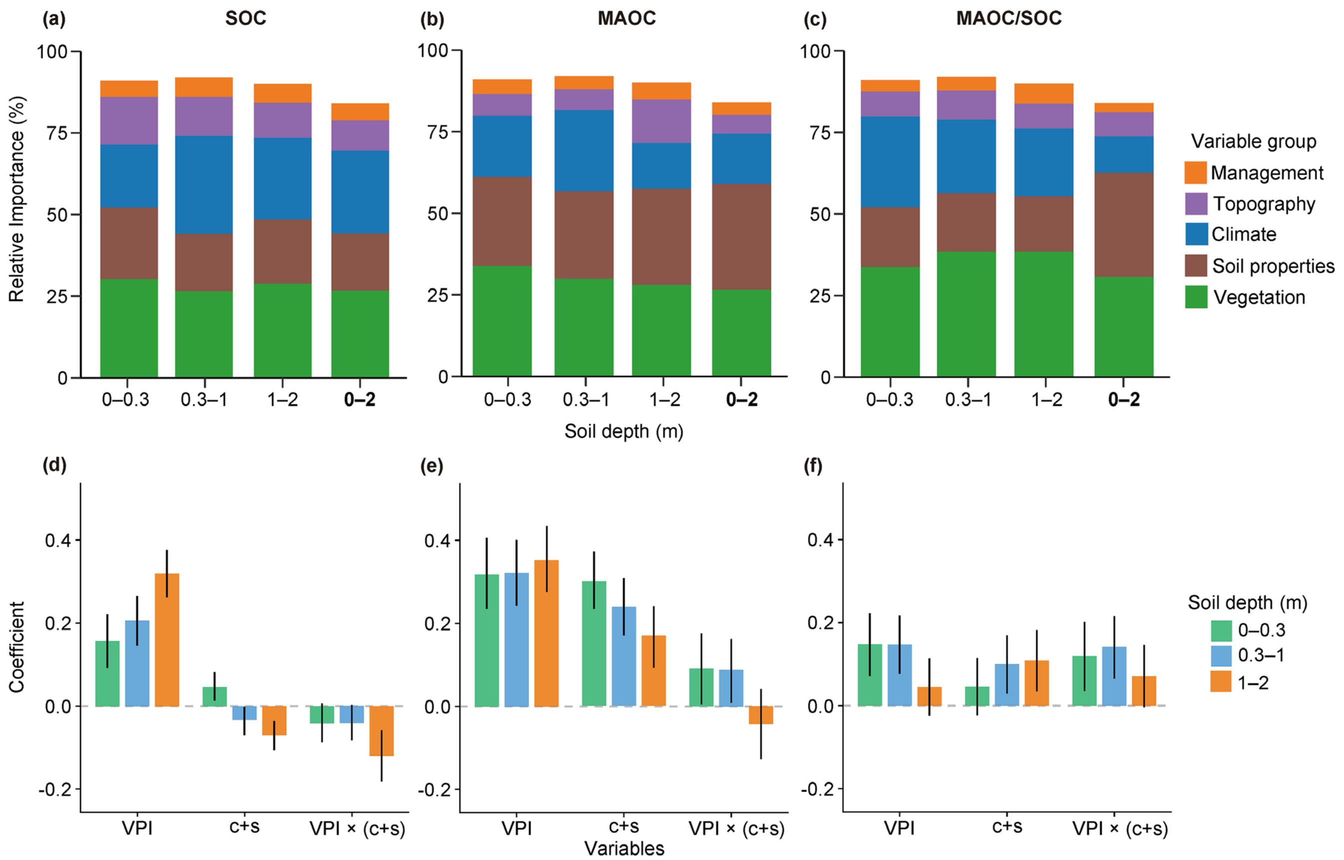

FIGURE 4 | Drivers of soil organic carbon and their depth-dependence. (a–c) Relative importance of five predictive variable groups (vegetation, soil properties, climate, topography, and management) in explaining total soil organic carbon (SOC, a), mineral-associated organic carbon (MAOC, b), and the MAOC/SOC ratio (c). (d–f) The effects (coefficients) of vegetation productivity index (VPI), clay + silt content (c + s), and their interaction on total soil organic carbon (SOC, d), mineral-associated organic carbon (MAOC, e), and their ratio MAOC/SOC (f) are estimated by a mixed-effects model driven by the standardized values of the three variables with soil profile (site) as a random effect. Error bars show the 95% confidence interval estimated as the 1.96 times the standard error of the coefficients.

processing, and thus MAOC formation (Prairie et al. 2023). Our findings are also consistent with recent evidence that diversifying cropping systems, such as cereal-legume intercropping, can increase and diversify belowground carbon inputs, enhance microbial processing, and promote the formation and persistence of mineral-associated organic carbon (Wang et al. 2025, 2026). Although our observational design does not allow the effects of specific cropping systems to be isolated, these studies provide a mechanistic framework for interpreting the positive relationship between vegetation productivity and MAOC observed in this study.

Other important predictors included elevation, fertilization rates, and crop yield, highlighting the combined influence of historical crop growth patterns and landscape features (Figure 3). Elevation, a proxy for landscape position and hydrological dynamics, influenced SOC through its regulation of erosion, deposition, and moisture conditions (Sanderman et al. 2017; Viscarra Rossel et al. 2019). Topographic processes could substantially influence MAOC distribution (e.g., MAOC enrichment in depositional zones) and MAOC/SOC ratios (e.g., lower ratios on erosional slopes) via particle-size sorting, parent material weathering, and mineral protection (Doetterl et al. 2016). Fertilization rates and crop yield positively influenced carbon variables, acting as proxies for carbon inputs and nutrient availability—two key determinants of microbial turnover and necromass stabilization (Sun et al. 2020; Zhao et al. 2018).

Contrary to global patterns where climate variables were dominant controls of SOC variability, individual climate predictors were less pronounced in our study region (Luo et al. 2021; Viscarra Rossel et al. 2019). This likely reflected the overriding effects of agricultural interventions such as irrigation and fertilization (which is particularly the case in China), which decoupled natural climate–SOC relationships in croplands (Lin et al. 2023). Nonetheless, climate extremes exerted relatively stronger impacts than normal climatic conditions, with icing days being the most influential climatic predictor (Figure 3). Icing days might restrict crop growth thereby reducing carbon inputs, and the associated freeze–thaw cycles can also physically disrupt soil aggregates and accelerate SOC decomposition (Lugato 2023).

Due to the leading importance of soil texture and vegetation dynamics, we further examined their relationships with the three carbon variables using linear mixed-effects models (Methods). To summarize vegetation signals, we constructed a vegetation productivity index (VPI) using principal component analysis of remote sensing variables (Table S3). Consistent with the RF results, both SOC and MAOC were strongly influenced by VPI and c + s, but their effects varied with depth (Figure 4d–f). For both SOC and MAOC, the positive effect of VPI intensified with depth, indicating an increasing dependence of subsoil carbon accumulation on fresh carbon inputs. In contrast, the effect of c + s diverged between carbon pools: its positive effect on MAOC weakened with depth, whereas its effect on SOC shifted from positive in surface soils to negative in deeper layers. These contrasting depth trends suggested that, although fine-textured soils favor MAOC formation, deep soil carbon accumulation is increasingly constrained by the supply of fresh carbon inputs rather than mineral capacity alone (Fontaine et al. 2007). Consistent with this interpretation, the MAOC/SOC ratio declined markedly with depth (Figure 1d) but remained positively associated with both VPI and c + s across the soil profile (Figure 4f), indicating that microbial processing of plant inputs and mineral interactions jointly promote MAOC formation.

Interactions between VPI and c+s further revealed depth-dependent controls on carbon stabilization (Figure 4d,e). For MAOC, the interaction was strongly positive in surface soils but weakened to near zero in deeper layers. In contrast, SOC showed consistently negative interactions that intensified with depth. Together, these patterns indicate a shift along the soil profile from joint mineral-input regulation near the surface toward increasingly input-limited carbon accumulation at depth. In surface soils, abundant plant inputs are most efficiently stabilized where mineral surfaces are abundant, generating strong positive interactions for MAOC. In deeper layers, where mineral surfaces are less saturated but carbon inputs are scarce, MAOC accumulation appears primarily constrained by the supply of fresh carbon inputs. Meanwhile, the negative interaction for total SOC suggests that fine-textured soils may dampen the positive effect of fresh carbon inputs, potentially because enhanced microbial processing and turnover offset part of the SOC gains from increased carbon inputs (Fontaine et al. 2007). Collectively, these results reveal depth-dependent trade-offs between carbon supply and mineral capacity in regulating SOC accumulation and stabilization.

3.3 | National Whole-Profile Carbon Stocks

We mapped 1 km-resolution SOC and MAOC stocks across three depth layers (0–0.3, 0.3–1, and 1–2 m) in Chinese dryland croplands (Methods, Figure 5). Cross-validated models yielded robust performance with R^2 values > 0.62 (Figures S5 and S6). We estimated national cropland SOC stocks at 19.9 Pg (95% confidence interval: 17.5–22.2 Pg) within the 0–2 m profile, corresponding to an average density of 189.79 t ha^{-1}. Of this, 75% resided below 0.3 m and 36% below 1 m (Table S4). By depth layer, SOC stocks were 5.0 Pg (4.4–5.6 Pg), 7.7 Pg (6.8–8.6 Pg), and 7.2 Pg (6.3–8.1 Pg), with corresponding densities of 47.7, 73.7, and 68.4 t ha^{-1} (Table S4). Among the nine agro-ecological regions, the Qinghai–Tibet Plateau exhibited the highest SOC density in the 0–2 m profile (294.7 t ha^{-1}), followed by the Yunnan–Guizhou Plateau (226.9 t ha^{-1}) and the Loess Plateau (224.8 t ha^{-1}, Table S5). These areas should be prioritized for SOC conservation in the study region. In contrast, the Huang–Huai–Hai Plain—the most intensively cultivated region in China—showed the lowest profile SOC density, indicating a critical need for restoration and sequestration efforts.

Comparison with existing SOC products including SoilGrids, WISE, HWSD (Methods) revealed systematic discrepancies. Our 0–0.3 m estimate (47.7 t ha^{-1}) closely matched WISE (48.7 t ha^{-1}), but exceeded those of SoilGrids and HWSD (Batjes 2016; FAO et al. 2012; Poggio et al. 2021; Table 2; Figure 6). Notably, global products predicted higher values in high-SOC regions (e.g., the Northeast China Plain) and lower values in low-SOC regions (e.g., the Huang–Huai–Hai Plain). For example, in the Northeast China Plain, SoilGrids reported 54.1 t ha^{-1} versus our 52.4 t ha^{-1}; while in the Huang–Huai–Hai Plain, SoilGrids reported 30.9 t ha^{-1} versus our 39.4 t ha^{-1} (Table S6). These discrepancies likely reflected differing data sources, sampling period, and mapping approaches. For example, a recent resampling study (1980 vs. 2023) showed a 0.7 Pg (7%) increase in topsoil SOC (0–0.6 m) across China's dryland croplands (Table S7), attributed to conservation policies such as residue retention and burning bans in the last decades (Qin et al. 2024; Zhou et al. 2025). Still, China's topsoil SOC remained substantially lower than that in other regions like European croplands (> 80 t ha^{-1}), probably due to millennia of intensive cultivation and the short duration of adopting conservation practices in recent decades (Lugato et al. 2014).

In the subsoil (0.3–1 m), our estimation of average SOC stock (73.7 t ha^{-1}) substantially exceeded estimates from other national studies (48–49 t ha^{-1}) and global datasets such as WISE (43.2 t ha^{-1}) and HWSD (42.8 t ha^{-1}), though it aligned more closely with SoilGrids (63.5 t ha^{-1}, Table S6; Tang et al. 2018; Zhang et al. 2025). Regional discrepancies were especially pronounced. For example, in the Loess Plateau, our subsoil estimate was 86.3 t ha^{-1}, compared to ~40 t ha^{-1} in all three global products (Table S6). Similar divergences persisted in the 1–2 m layer, where our estimate (68.4 t ha^{-1}) was lower than SoilGrids (75.6 t ha^{-1}) but higher than WISE (37.3 t ha^{-1}). At the regional scale, the Northern Arid and Semi-arid Region held the largest total SOC stock (5.2 Pg in 0–2 m), followed by the Huang–Huai–Hai Plain (3.7 Pg), largely reflecting its vast cropland area (Table S5).

Estimated MAOC stocks were 3.1 Pg (1.8–4.4 Pg), 4.9 Pg (2.1–7.8 Pg), and 3.9 Pg (1.0–5.0 Pg) across the three depth layers (Table S4), comprising 62%, 64%, and 54% of total SOC, respectively. This indicated that approximately 40% of SOC existed as more labile forms (e.g., particulate organic carbon), particularly in deeper layers. Given the higher sensitivity of particulate organic carbon to disturbance and climate change, especially in high-stock areas like the Northeast China Plain, proactive management is essential to mitigate potential losses (Lugato et al. 2021). On average, MAOC densities were 29.3, 46.7, and 37.3 t ha^{-1}, with ~75% residing below 0.3 m. Compared to global averages (e.g., 43.1 t ha^{-1} in 0–0.3 m), Chinese croplands stored less MAOC (Georgiou et al. 2022). Regional discrepancies were again evident. Georgiou et al. (2022) estimated 63.7 t ha^{-1} in the 0.3–1 m layer of the Northern Arid and Semi-arid Region, more than our estimate of 56.6 t ha^{-1} (Figure S7). Despite these differences, regional patterns of MAOC closely mirrored those of SOC (Figure 5). The Northern Arid and Semi-arid Region and the Northeast China Plain harbored the highest 0–2 m MAOC stocks (3.1 and 2.8 Pg, respectively), while the Qinghai–Tibet Plateau showed the lowest (0.1 Pg).

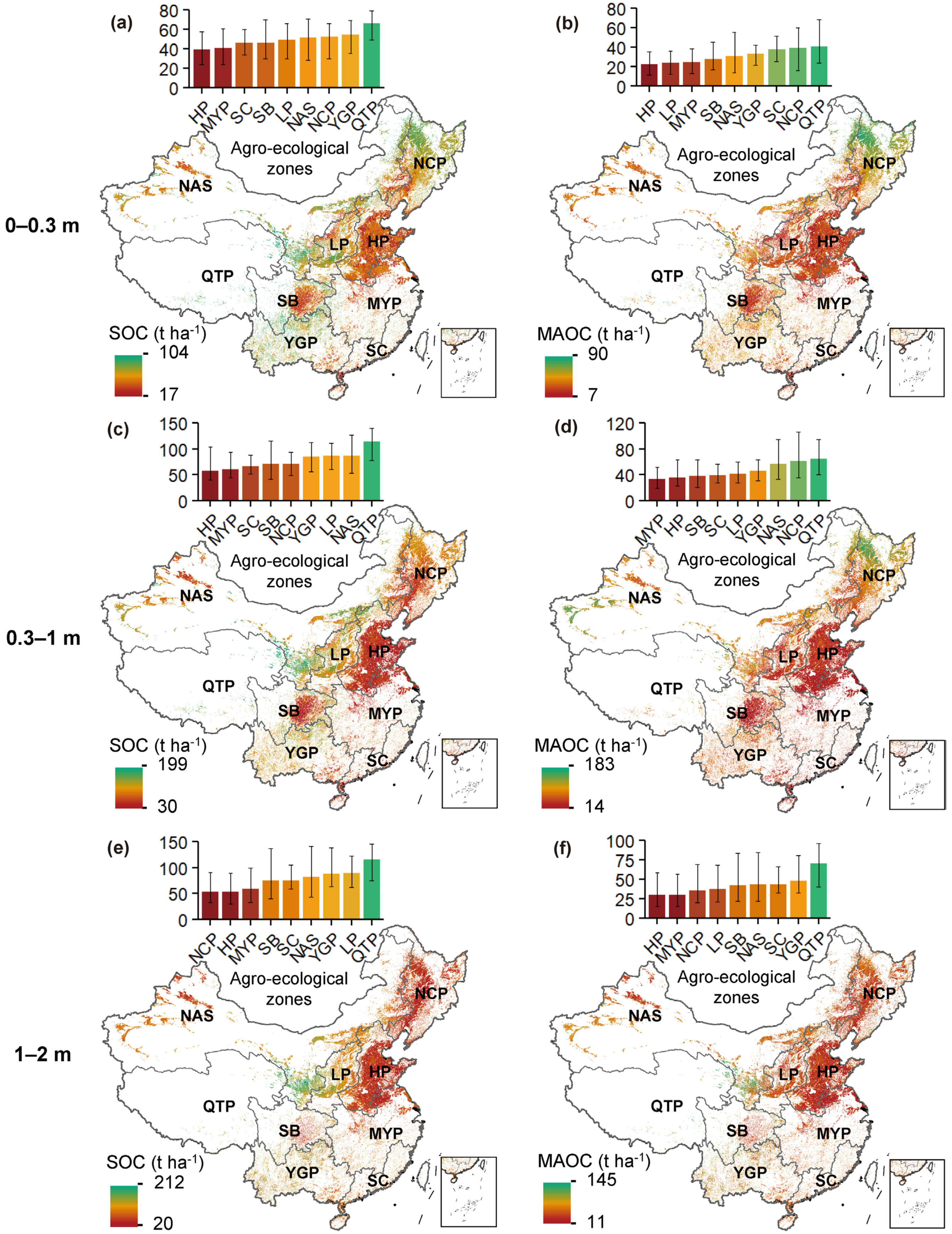

FIGURE 5 | Legend on next page.

FIGURE 5 | Spatial patterns of soil carbon stocks. Left (a, c, e) and right (b, d, f) panels show total soil organic carbon (SOC) and mineral-associated organic carbon (MAOC) stocks in three depth layers, respectively. Barplots above each map show the relevant average stocks in nine agro-ecological zones in China (HP, Huang–Huai–Hai Plain; LP, Loess Plateau; MYP, Middle-lower Yangtze Plain; NAS, Northern arid and Semi-arid region; NCP, Northeast China Plain; QTP, Qinghai–Tibet Plateau; SB, Sichuan Basin; SC, Southern China; YGP, Yunnan–Guizhou Plateau) in order of magnitude, with error bars representing the 95% confidence intervals (i.e., 2.5% and 97.5% quantiles).

TABLE 2 | Comparison of estimated national stocks of soil organic carbon (SOC) in Chinese dryland croplands in the present study, SoilGrids, WISE, and HWSD (Batjes 2016; FAO et al. 2012; Poggio et al. 2021).

	Present study		SoilGrids		WISE		HWSD	
Depth (m)	SOC density ($t\,ha^{-1}$)	SOC stock (Pg)	SOC density ($t\,ha^{-1}$)	SOC stock (Pg)	SOC density ($t\,ha^{-1}$)	SOC stock (Pg)	SOC density ($t\,ha^{-1}$)	SOC stock (Pg)
0–0.3	47.7	5.0	42.9	4.5	48.7	5.1	38.3	4.0
0.3–1	73.7	7.7	63.5	6.7	43.2	4.5	42.8	4.5
1–2	68.4	7.2	75.6	7.9	37.3	3.9	—	—
0–2	189.8	19.9	182.0	19.1	129.2	13.6	—	—

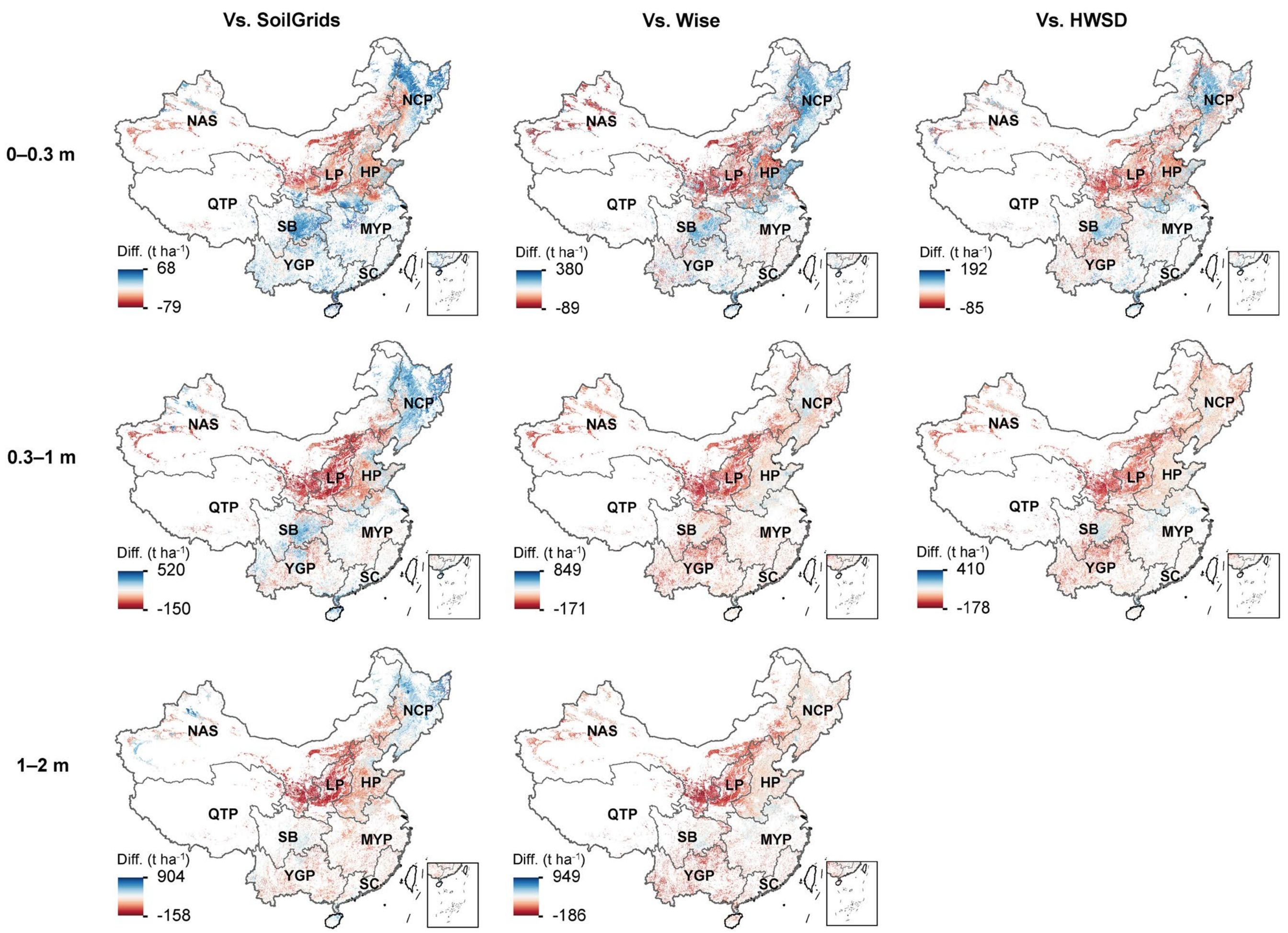

FIGURE 6 | Comparison of soil organic carbon (SOC) stocks estimated in this study to global mapping products in Chinese dryland croplands. Each grid cell displays the difference between SOC estimates from global databases (SoilGrids, WISE, or HWSD, Methods) and our mapping results (Figure 5) across depth layers. Blue cells denote higher values in the reference databases relative to this study, while red cells indicate lower estimates.

4 | Implications and Conclusion

This study provides a nationwide, observation-based assessment of the vertical distribution of soil organic carbon (SOC) and its mineral-associated fraction (MAOC) across dryland croplands in China to 2 m depth. Contrary to the commonly assumed exponential decline of SOC with depth, nearly half of the sampled profiles exhibited relatively uniform or even increasing SOC and MAOC stocks with depth. These patterns highlight the substantial but often overlooked contribution of subsoil carbon, with approximately three quarters of total SOC stored below 0.3 m in these systems. At the same time, the proportion of SOC associated with minerals declined in deeper layers, indicating that a considerable fraction of subsoil carbon occurs in less mineral-protected pools. Profiles in which MAOC increased with depth were largely confined to the arid and semi-arid north, whereas increasing MAOC/SOC ratios occurred more widely, including the Qinghai-Tibet, Loess Plateaus, and parts of the northern plains (Figure S2). Across profiles, increasing MAOC and MAOC/SOC with depth were positively associated with increasing clay + silt content, indicating that greater mineral surface availability in subsoils promoted organo-mineral stabilization. In regions where clay + silt content changed little with depth, regional difference in mineralogy and the slower decomposition associated with arid climates may also help enhance subsoil carbon stabilization, although these mechanisms were not directly evaluated here. Together, these findings suggest that depth-dependent variation in mineral capacity, together with regional environmental conditions, contributes to the observed heterogeneity in MAOC distribution across China.

Across the soil profile, soil texture and vegetation productivity emerged as the dominant predictors of SOC and MAOC. Fine particle content (clay + silt) was consistently associated with greater SOC and MAOC stocks, reflecting the well-established role of mineral surface in promoting organo-mineral interactions and microbial residue stabilization (Georgiou et al. 2022). Soils with higher clay + silt content support greater organo-mineral associations and offer higher potential for long-term carbon sequestration (Georgiou et al. 2022). Vegetation productivity, captured through satellite-derived indicators, provided an integrative proxy for carbon inputs from crop growth and cropping intensity. Together, these results emphasize that both the supply of organic substrates and the availability of mineral surfaces are fundamental constraints on soil carbon accumulation. Importantly, the influence of these controls varied systematically with depth. Indicators of vegetation productivity showed increasingly strong relationships with SOC and MAOC in deeper soils, whereas the influence of fine particle content weakened for MAOC and shifted for total SOC. These patterns indicate that carbon stabilization mechanisms change along the soil profile. In surface soils, where carbon inputs are abundant, mineral surfaces and substrate supply jointly regulate the formation of mineral-associated carbon. In deeper horizons, where mineral surfaces are relatively unsaturated but fresh inputs are scarce, carbon accumulation appears increasingly constrained by the availability of organic substrates. This depth-dependent shift suggests that subsoil carbon dynamics are governed less by mineral capacity than by the magnitude and vertical distribution of plant-derived inputs.

The spatially explicit estimates of whole-profile SOC and MAOC stocks presented here provide a benchmark for evaluating soil carbon storage in one of the world's largest agricultural regions. Our results also highlight strong regional contrasts in carbon storage, with northern dryland cropland regions containing a large proportion of national MAOC stocks. Protecting these high-carbon soils is therefore important for maintaining existing carbon reservoirs, particularly under warming climates and continued agricultural intensification. Additionally, these regional contrasts in carbon storage may partly reflect differences in cropping and tillage practices. Across the sampled croplands, maize-containing systems dominated, comprising summer maize monoculture (36% of sites) and winter wheat–summer maize rotation (49%), while management was primarily conventional tillage (54%), with no-till and rotary tillage accounting for 28% and 18% of sites, respectively. These systems showed regional patterns: maize-based cropping with widespread conservation tillage characterized the Northeast China Plain, whereas winter wheat–summer maize rotations dominated the Huang–Huai–Hai Plain and conventional tillage prevailed across most other regions. Because these management practices co-vary strongly with regional climate and soil properties, their effects are difficult to separate from environmental controls in this observational study and are therefore interpreted as acting in concert with them.

However, we would also like to highlight several limitations. Although our dataset provides extensive depth-resolved observations across China's dryland croplands, the sampling density remains limited relative to the large spatial extent and heterogeneity of the study region. More extensive sampling would certainly be valuable, particularly for improving mapping accuracy of stocks of SOC and its fractions. Moreover, complementary measurements of particulate organic carbon, soil inorganic carbon, dissolved organic carbon, and reactive Fe and Al (hydr)oxides would further strengthen mechanistic interpretation of the observed vertical SOC and MAOC patterns, particularly in arid and semi-arid regions where carbonate accumulation and mineralogical controls may be important. Similarly, key nutrients such as nitrogen and phosphorus are tightly coupled with soil carbon cycling, and their concentrations, stoichiometric balance (e.g., C:N:P ratios), and chemical forms may regulate the formation, stabilization, and persistence of SOC and MAOC. Future incorporation of these nutrient dimensions, together with quantitative, depth-resolved measurements of carbon inputs (e.g., root biomass, root turnover, and rhizodeposition), would help refine attribution of SOC and MAOC drivers and provide a more mechanistic understanding of whole-profile carbon stabilization.

Together, these findings demonstrate that soil carbon storage and stabilization are inherently depth dependent. Carbon inputs primarily determine the magnitude of SOC accumulation, while mineral surfaces regulate the extent to which this carbon is stabilized as MAOC. Although derived from Chinese dryland croplands, the depth-dependent transition identified here likely applies broadly to intensively managed agricultural soils where subsoil carbon inputs are limited. Effective soil carbon management and modeling efforts should explicitly consider the vertical structure of soils and the interacting roles of organic inputs and mineralogical constraints. Aligning carbon inputs with the stabilization capacity of soils across depth may represent an important pathway for enhancing long-term soil carbon storage in agricultural landscapes.

Author Contributions

Hong Chen: writing – review and editing. **Jinfeng Chang:** investigation, writing – review and editing. **Zhou Shi:** investigation, writing – review and editing. **Yuchen Wei:** conceptualization, data curation, methodology, investigation, validation, formal analysis, visualization, writing – original draft, software. **Wenting Feng:** data curation, investigation, writing – review and editing. **Xin Zhao:** data curation, writing – review and editing, investigation. **Xiaowei Guo:** data curation, investigation, writing – review and editing. **Zhaoliang Song:** writing – review and editing. **Raphael A. Viscarra Rossel:** writing – review and editing. **Hongyong Sun:** data curation, investigation, writing – review and editing. **Alain F. Plante:** writing – review and editing. **Enli Wang:** writing – review and editing. **Mingming Wang:** investigation, writing – review and editing. **Liujun Xiao:** investigation, writing – review and editing. **Lewis Walden:** writing – review and editing. **Shuai Zhang:** investigation, writing – review and editing. **Hangxin Zhou:** investigation. **Feng Liu:** resources. **Su Ye:** software, writing – review and editing. **Ji Chen:** writing – review and editing. **Zhongkui Luo:** conceptualization, methodology, supervision, funding acquisition, project administration, writing – review and editing, resources. **Di He:** writing – review and editing.

Acknowledgments

We thank all farmers involved in the field survey and their support for the soil sampling, and Jingyang Zheng, Tian Qian, Tong Jiang, Yin Lin, and Mingxuan Qi for their help on soil sampling.

Funding

This work was financially supported by the Natural Science Foundation of Zhejiang Province (LZ25D030001). National Natural Science Foundation of China (32241036, 42225101). Fundamental and Interdisciplinary Disciplines Breakthrough Plan of the Ministry of Education of China (JYB2025XDXM909).

Conflicts of Interest

The authors declare no conflicts of interest.

Data Availability Statement

The data that support the findings of this study are available in Figshare at https://doi.org/10.6084/m9.figshare.33138044. The global and national gridded datasets used in this study as environmental covariates are available in the public domain (see Table S2 for a full list). All the code used in the analyses presented in this paper is available via https://doi.org/10.6084/m9.figshare.28352600.

References

Alexander, L. V. 2016. "Global Observed Long-Term Changes in Temperature and Precipitation Extremes: A Review of Progress and Limitations in IPCC Assessments and Beyond." *Weather and Climate Extremes* 11: 4–16. https://doi.org/10.1016/j.wace.2015.10.007.

Batjes, N. H. 2016. "Harmonized Soil Property Values for Broad-Scale Modelling (WISE30sec) With Estimates of Global Soil Carbon Stocks." *Geoderma* 269: 61–68. https://doi.org/10.1016/j.geoderma.2016.01.034.

Bernal, B., D. C. McKinley, B. A. Hungate, P. M. White, T. J. Mozdzer, and J. P. Megonigal. 2016. "Limits to Soil Carbon Stability; Deep, Ancient Soil Carbon Decomposition Stimulated by New Labile Organic Inputs." *Soil Biology & Biochemistry* 98: 85–94. https://doi.org/10.1016/j.soilbio.2016.04.007.

Breiman, L. 2001. "Random Forests." *Machine Learning* 45, no. 1: 5–32. https://doi.org/10.1023/A:1010933404324.

Button, E. S., J. Pett-Ridge, D. V. Murphy, Y. Kuzyakov, D. R. Chadwick, and D. L. Jones. 2022. "Deep-C Storage: Biological, Chemical and Physical Strategies to Enhance Carbon Stocks in Agricultural Subsoils." *Soil Biology & Biochemistry* 170: 108697. https://doi.org/10.1016/j.soilbio.2022.108697.

Conrad, O., B. Bechtel, M. Bock, et al. 2015. "System for Automated Geoscientific Analyses (SAGA) v. 2.1.4." *Geoscientific Model Development* 8, no. 7: 1991–2007. https://doi.org/10.5194/gmd-8-1991-2015.

Cotrufo, M. F., M. G. Ranalli, M. L. Haddix, J. Six, and E. Lugato. 2019. "Soil Carbon Storage Informed by Particulate and Mineral-Associated Organic Matter." *Nature Geoscience* 12, no. 12: 989–994. https://doi.org/10.1038/s41561-019-0484-6.

Department of Rural Social and Economic Survey of the National Bureau of Statistics of China. 2023. *China County Statistical Yearbook 2023 (Township Volume) [in Chinese]*. China Statistics Press Co., Ltd.

Dialynas, Y. G., S. Bastola, R. L. Bras, S. A. Billings, D. Markewitz, and D. D. Richter. 2016. "Topographic Variability and the Influence of Soil Erosion on the Carbon Cycle." *Global Biogeochemical Cycles* 30, no. 5: 644–660. https://doi.org/10.1002/2015gb005302.

Doetterl, S., A. A. Berhe, E. Nadeu, Z. G. Wang, M. Sommer, and P. Fiener. 2016. "Erosion, Deposition and Soil Carbon: A Review of Process-Level Controls, Experimental Tools and Models to Address C Cycling in Dynamic Landscapes." *Earth-Science Reviews* 154: 102–122. https://doi.org/10.1016/j.earscirev.2015.12.005.

FAO, IIASA, ISRIC, ISSCAS, and JRC. 2012. *Harmonized World Soil Database (version 1.2)* Retrieved from Rome, Italy and Laxenburg, Austria.

Fick, S. E., and R. J. Hijmans. 2017. "WorldClim 2: New 1-Km Spatial Resolution Climate Surfaces for Global Land Areas." *International Journal of Climatology* 37, no. 12: 4302–4315. https://doi.org/10.1002/joc.5086.

Fontaine, S., S. Barot, P. Barré, N. Bdioui, B. Mary, and C. Rumpel. 2007. "Stability of Organic Carbon in Deep Soil Layers Controlled by Fresh Carbon Supply." *Nature* 450, no. 7167: 277–280. https://doi.org/10.1038/nature06275.

Fox, J., and S. Weisberg. 2019. *An R Companion to Applied Regression*. 3rd ed. Sage.

Garland, G., A. Edlinger, S. Banerjee, et al. 2021. "Crop Cover Is More Important Than Rotational Diversity for Soil Multifunctionality and Cereal Yields in European Cropping Systems." *Nature Food* 2, no. 1: 28–37. https://doi.org/10.1038/s43016-020-00210-8.

Georgiou, K., R. B. Jackson, O. Vindušková, et al. 2022. "Global Stocks and Capacity of Mineral-Associated Soil Organic Carbon." *Nature Communications* 13, no. 1: 3797. https://doi.org/10.1038/s41467-022-31540-9.

Henneron, L., J. Balesdent, G. Alvarez, et al. 2022. "Bioenergetic Control of Soil Carbon Dynamics Across Depth." *Nature Communications* 13, no. 1: 7676. https://doi.org/10.1038/s41467-022-34951-w.

Hijmans, R. J., S. E. Cameron, J. L. Parra, P. G. Jones, and A. Jarvis. 2005. "Very High Resolution Interpolated Climate Surfaces for Global Land Areas." *International Journal of Climatology* 25, no. 15: 1965–1978. https://doi.org/10.1002/joc.1276.

Ito, A., and R. Wagai. 2017. "Global Distribution of Clay-Size Minerals on Land Surface for Biogeochemical and Climatological Studies." *Scientific Data* 4: 170103. https://doi.org/10.1038/sdata.2017.103.

Jobbágy, E. G., and R. B. Jackson. 2000. "The Vertical Distribution of Soil Organic Carbon and Its Relation to Climate and Vegetation." *Ecological Applications* 10, no. 2: 423–436. https://doi.org/10.2307/2641104.

Kleber, M., K. Eusterhues, M. Keiluweit, C. Mikutta, R. Mikutta, and P. S. Nico. 2015. "Mineral-Organic Associations: Formation, Properties, and Relevance in Soil Environments." *Advances in Agronomy* 130: 1–140. https://doi.org/10.1016/bs.agron.2014.10.005.

Kuhn, M. 2008. "Building Predictive Models in R Using the Caret Package." *Journal of Statistical Software* 28, no. 5: 1–26. https://doi.org/10.18637/jss.v028.i05.

Kuznetsova, A., P. B. Brockhoff, and R. H. B. Christensen. 2017. "lmerTest Package: Tests in Linear Mixed Effects Models." *Journal of Statistical Software* 82, no. 13: 1–26. https://doi.org/10.18637/jss.v082.i13.

Lal, R. 2004. "Soil Carbon Sequestration Impacts on Global Climate Change and Food Security." *Science* 304, no. 5677: 1623–1627. https://doi.org/10.1126/science.1097396.

Lavallee, J. M., J. L. Soong, and M. F. Cotrufo. 2020. "Conceptualizing Soil Organic Matter Into Particulate and Mineral-Associated Forms to Address Global Change in the 21st Century." *Global Change Biology* 26, no. 1: 261–273. https://doi.org/10.1111/gcb.14859.

Leading Group Office of the State Council for the Third National Land Survey, Ministry of Natural Resources of the People's Republic of China, and National Bureau of Statistics of China. 2023. "Main Data Bulletin of the Third National Land Survey [in Chinese]." https://www.mnr.gov.cn/dt/ywbb/202108/t20210826_2678340.html.

Li, Q. L., G. S. Shi, W. Shangguan, et al. 2022. "A 1 Km Daily Soil Moisture Dataset Over China Using In Situ Measurement and Machine Learning." *Earth System Science Data* 14, no. 12: 5267–5286. https://doi.org/10.5194/essd-14-5267-2022.

Liang, C., W. Amelung, J. Lehmann, and M. Kästner. 2019. "Quantitative Assessment of Microbial Necromass Contribution to Soil Organic Matter." *Global Change Biology* 25, no. 11: 3578–3590. https://doi.org/10.1111/gcb.14781.

Liebmann, P., P. Wordell-Dietrich, K. Kalbitz, et al. 2020. "Relevance of Aboveground Litter for Soil Organic Matter Formation - a Soil Profile Perspective." *Biogeosciences* 17, no. 12: 3099–3113. https://doi.org/10.5194/bg-17-3099-2020.

Lin, B. J., R. C. Li, K. C. Liu, et al. 2023. "Management-Induced Changes in Soil Organic Carbon and Related Crop Yield Dynamics in China's Cropland." *Global Change Biology* 29, no. 13: 3575–3590. https://doi.org/10.1111/gcb.16703.

Liu, J. H., W. Q. Zhu, C. Atzberger, A. Z. Zhao, Y. Z. Pan, and X. Huang. 2018. "A Phenology-Based Method to Map Cropping Patterns Under a Wheat-Maize Rotation Using Remotely Sensed Time-Series Data." *Remote Sensing* 10, no. 8: 1203. https://doi.org/10.3390/rs10081203.

Liu, M. L., S. L. Zheng, E. Pendall, et al. 2025. "Unprotected Carbon Dominates Decadal Soil Carbon Increase." *Nature Communications* 16, no. 1: 2008. https://doi.org/10.1038/s41467-025-57354-z.

Liu, Y. D., Y. N. Huang, B. S. Ndzelu, and R. X. Hou. 2025. "Carbon Saturation Level Regulates the Stability of Mineral-Associated Organic Carbon in Forest Soils." *Catena* 259: 109391. https://doi.org/10.1016/j.catena.2025.109391.

Lugato, E. 2023. "Soil Organic Carbon Losses Exacerbated by Climate Extremes." *Nature Climate Change* 14: 17–18. https://doi.org/10.1038/s41558-023-01873-4.

Lugato, E., J. M. Lavallee, M. L. Haddix, P. Panagos, and M. F. Cotrufo. 2021. "Different Climate Sensitivity of Particulate and Mineral-Associated Soil Organic Matter." *Nature Geoscience* 14, no. 5: 295–300. https://doi.org/10.1038/s41561-021-00744-x.

Lugato, E., P. Panagos, F. Bampa, A. Jones, and L. Montanarella. 2014. "A New Baseline of Organic Carbon Stock in European Agricultural Soils Using a Modelling Approach." *Global Change Biology* 20, no. 1: 313–326. https://doi.org/10.1111/gcb.12292.

Luo, Z., E. Wang, and O. J. Sun. 2010. "Soil Carbon Change and Its Responses to Agricultural Practices in Australian Agro-Ecosystems: A Review and Synthesis." *Geoderma* 155, no. 3–4: 211–223. https://doi.org/10.1016/j.geoderma.2009.12.012.

Luo, Z. K. 2025. "Big Soil Benefits From Buried Straw." *Nature Geoscience* 18, no. 7: 570–571. https://doi.org/10.1038/s41561-025-01732-1.

Luo, Z. K., R. A. Viscarra-Rossel, and T. Qian. 2021. "Similar Importance of Edaphic and Climatic Factors for Controlling Soil Organic Carbon Stocks of the World." *Biogeosciences* 18, no. 6: 2063–2073. https://doi.org/10.5194/bg-18-2063-2021.

Luo, Z. K., M. M. Wang, and G. C. Wang. 2025. "Unlocking the Potential of Whole-Profile Carbon Sequestration in Agricultural Soils." *Frontiers in Earth Science* 20: 39–47. https://doi.org/10.1007/s11707-025-1168-8.

Malone, B. P., A. B. McBratney, B. Minasny, and G. M. Laslett. 2009. "Mapping Continuous Depth Functions of Soil Carbon Storage and Available Water Capacity." *Geoderma* 154, no. 1: 138–152. https://doi.org/10.1016/j.geoderma.2009.10.007.

Mistry, M. N. 2019. "A High-Resolution Global Gridded Historical Dataset of Climate Extreme Indices." *Data* 4, no. 1: 41. https://doi.org/10.3390/data4010041.

Orgiazzi, A., C. Ballabio, P. Panagos, A. Jones, and O. Fernández-Ugalde. 2018. "LUCAS Soil, the Largest Expandable Soil Dataset for Europe: A Review." *European Journal of Soil Science* 69, no. 1: 140–153. https://doi.org/10.1111/ejss.12499.

Poggio, L., L. M. de Sousa, N. H. Batjes, et al. 2021. "SoilGrids 2.0: Producing Soil Information for the Globe With Quantified Spatial Uncertainty." *Soil* 7, no. 1: 217–240. https://doi.org/10.5194/soil-7-217-2021.

Prairie, A. M., A. E. King, and M. F. Cotrufo. 2023. "Restoring Particulate and Mineral-Associated Organic Carbon Through Regenerative Agriculture." *Proceedings of the National Academy of Sciences of the United States of America* 120, no. 21: e2217481120. https://doi.org/10.1073/pnas.2217481120.

Pries, C. E. H., R. Ryals, B. Zhu, et al. 2023. "The Deep Soil Organic Carbon Response to Global Change." *Annual Review of Ecology, Evolution, and Systematics* 54: 375–401. https://doi.org/10.1146/annurev-ecolsys-102320-085332.

Qin, W. F., L. L. Niu, Y. L. You, S. Cui, C. Chen, and Z. Li. 2024. "Effects of Conservation Tillage and Straw Mulching on Crop Yield, Water Use Efficiency, Carbon Sequestration and Economic Benefits in the Loess Plateau Region of China: A Meta-Analysis." *Soil & Tillage Research* 238: 106025. https://doi.org/10.1016/j.still.2024.106025.

R Core Team. 2013. *R: A Language and Environment for Statistical Computing.* R Foundation for Statistical Computing.

Rodell, M., P. R. Houser, U. Jambor, et al. 2004. "The Global Land Data Assimilation System." *Bulletin of the American Meteorological Society* 85, no. 3: 381–394. https://doi.org/10.1175/Bams-85-3-381.

Rumpel, C., and I. Kögel-Knabner. 2011. "Deep Soil Organic Matter—A Key but Poorly Understood Component of Terrestrial C Cycle." *Plant and Soil* 338: 143–158.

Sanderman, J., T. Hengl, and G. J. Fiske. 2017. "Soil Carbon Debt of 12,000 Years of Human Land Use." *Proceedings. National Academy of Sciences. United States of America* 114, no. 36: 9575–9580. https://doi.org/10.1073/pnas.1706103114.

Schweizer, S. A., C. W. Mueller, C. Höschen, P. Ivanov, and I. Kögel-Knabner. 2021. "The Role of Clay Content and Mineral Surface Area for Soil Organic Carbon Storage in an Arable Toposequence." *Biogeochemistry* 156, no. 3: 401–420. https://doi.org/10.1007/s10533-021-00850-3.

Shangguan, W., Y. J. Dai, B. Y. Liu, et al. 2013. "A China Data Set of Soil Properties for Land Surface Modeling." *Journal of Advances in Modeling Earth Systems* 5, no. 2: 212–224. https://doi.org/10.1002/jame.20026.

Sierra, C. A., B. Ahrens, M. A. Bolinder, et al. 2024. "Carbon Sequestration in the Subsoil and the Time Required to Stabilize Carbon for Climate Change Mitigation." *Global Change Biology* 30, no. 1: e17153. https://doi.org/10.1111/gcb.17153.

Six, J., R. T. Conant, E. A. Paul, and K. Paustian. 2002. "Stabilization Mechanisms of Soil Organic Matter: Implications for C-Saturation of Soils." *Plant and Soil* 241, no. 2: 155–176. https://doi.org/10.1023/A:1016125726789.

Sokol, N. W., and M. A. Bradford. 2019. "Microbial Formation of Stable Soil Carbon Is More Efficient From Belowground Than Aboveground Input." *Nature Geoscience* 12, no. 1: 46–53. https://doi.org/10.1038/s41561-018-0258-6.

Sun, W. J., J. G. Canadell, L. J. Yu, et al. 2020. "Climate Drives Global Soil Carbon Sequestration and Crop Yield Changes Under Conservation Agriculture." *Global Change Biology* 26, no. 6: 3325–3335. https://doi.org/10.1111/gcb.15001.

Tang, G. 2019. "Digital elevation model of China (1 km)." https://data.tpdc.ac.cn/en/data/12e91073-0181-44bf-8308-c50e5bd9a734.

Tang, X. L., X. Zhao, Y. F. Bai, et al. 2018. "Carbon Pools in China's Terrestrial Ecosystems: New Estimates Based on an Intensive Field Survey." *Proceedings of the National Academy of Sciences of the United States of America* 115, no. 16: 4021–4026. https://doi.org/10.1073/pnas.1700291115.

Torn, M. S., S. E. Trumbore, O. A. Chadwick, P. M. Vitousek, and D. M. Hendricks. 1997. "Mineral Control of Soil Organic Carbon Storage and Turnover." *Nature* 389, no. 6647: 170–173. https://doi.org/10.1038/38260.

Viscarra Rossel, R. A., J. Lee, T. Behrens, Z. Luo, J. Baldock, and A. Richards. 2019. "Continental-Scale Soil Carbon Composition and Vulnerability Modulated by Regional Environmental Controls." *Nature Geoscience* 12, no. 7: 547–552. https://doi.org/10.1038/s41561-019-0373-z.

Wang, D., A. H. Wang, and Z. Q. Wang. 2023. "A Multilayer Daily High-Resolution Gridded Homogenized Soil Temperature Over Continental China." *International Journal of Climatology* 43, no. 5: 2015–2030. https://doi.org/10.1002/joc.7959.

Wang, W., M.-Y. Li, Q.-H. Wen, et al. 2025. "Cereal-Legume Intercropping Stimulates Straw Decomposition and Promotes Soil Organic Carbon Stability." *Science China Life Sciences* 68, no. 5: 1498–1508. https://doi.org/10.1007/s11427-024-2683-y.

Wang, W., Y. Wang, J.-M. Li, et al. 2026. "Long-Term Intercropping Mitigates Warming-Induced Carbon Loss via Enhancing Microbial and Substrate Resistance." *Soil Biology and Biochemistry* 212: 110022. https://doi.org/10.1016/j.soilbio.2025.110022.

Wang, Y. Q., M. A. Shao, C. C. Zhang, Z. P. Liu, J. L. Zou, and J. F. Xiao. 2015. "Soil Organic Carbon in Deep Profiles Under Chinese Continental Monsoon Climate and Its Relations With Land Uses." *Ecological Engineering* 82: 361–367. https://doi.org/10.1016/j.ecoleng.2015.05.004.

Weng, Z., L. Van Zwieten, B. P. Singh, et al. 2017. "Biochar Built Soil Carbon Over a Decade by Stabilizing Rhizodeposits." *Nature Climate Change* 7, no. 5: 371–376. https://doi.org/10.1038/nclimate3276.

Wilson, B. T., J. F. Knight, and R. E. McRoberts. 2018. "Harmonic Regression of Landsat Time Series for Modeling Attributes From National Forest Inventory Data." *ISPRS Journal of Photogrammetry and Remote Sensing* 137: 29–46. https://doi.org/10.1016/j.isprsjprs.2018.01.006.

Wright, M. N., and A. Ziegler. 2017. "Ranger: A Fast Implementation of Random Forests for High Dimensional Data in C++ and R." *Journal of Statistical Software* 77, no. 1: 1–17. https://doi.org/10.18637/jss.v077.i01.

Yu, Z., J. Liu, and G. Kattel. 2022. "Historical Nitrogen Fertilizer Use in China From 1952 to 2018." *Earth System Science Data* 14, no. 11: 5179–5194. https://doi.org/10.5194/essd-14-5179-2022.

Zhang, S. H., Y. S. Chen, X. B. Zhou, and B. Zhu. 2025. "Spatial Distribution, Drivers and Future Trends of Soil Organic Carbon in Cropland of China." *Soil Science Society of America Journal* 89, no. 2: e70042. https://doi.org/10.1002/saj2.70042.

Zhang, Y. Q., D. D. Kong, R. Gan, et al. 2019. "Coupled Estimation of 500 m and 8-Day Resolution Global Evapotranspiration and Gross Primary Production in 2002-2017." *Remote Sensing of Environment* 222: 165–182. https://doi.org/10.1016/j.rse.2018.12.031.

Zhao, Y. C., M. Y. Wang, S. J. Hu, et al. 2018. "Economics- and Policy-Driven Organic Carbon Input Enhancement Dominates Soil Organic Carbon Accumulation in Chinese Croplands." *Proceedings of the National Academy of Sciences of the United States of America* 115, no. 16: 4045–4050. https://doi.org/10.1073/pnas.1700292114.

Zhou, Z., C. Ren, C. Wang, et al. 2024. "Global Turnover of Soil Mineral-Associated and Particulate Organic Carbon." *Nature Communications* 15, no. 1: 5329. https://doi.org/10.1038/s41467-024-49743-7.

Zhou, Z. H., C. K. Wang, Y. E. Li, et al. 2025. "Carbon Gain in Upper but Loss in Deeper Cropland Soils Across China Over the Last Four Decades." *Proceedings of the National Academy of Sciences of the United States of America* 122, no. 1: e2422371122. https://doi.org/10.1073/pnas.2422371122.

Zhu, Z., and C. E. Woodcock. 2014. "Continuous Change Detection and Classification of Land Cover Using All Available Landsat Data." *Remote Sensing of Environment* 144: 152–171. https://doi.org/10.1016/j.rse.2014.01.011.

Supporting Information

Additional supporting information can be found online in the Supporting Information section. **Figure S1:** Frequency distribution of soil organic carbon. Frequency distribution curves are shown for (a) total soil organic carbon (SOC), (b) mineral-associated organic carbon (MAOC), and (c) the ratio of MAOC to SOC (MAOC/SOC). Different colors represent soil depth layers. **Figure S2:** Vertical distribution patterns of soil organic carbon in nine agro-ecological zones of China. (a) total soil organic carbon (SOC), (b) mineral-associated organic carbon (MAOC), (c) the ratio of MAOC to SOC (MAOC/SOC). Agro-ecological zones are shown as: NCP, Northeast China Plain; NAS, Northern arid and Semi-arid region; HP, Huang–Huai–Hai Plain; LP, Loess Plateau; QTP, Qinghai–Tibet Plateau; MYP, Middle-lower Yangtze Plain; SB, Sichuan Basin and surrounding regions; YGP, Yunnan–Guizhou Plateau; SC, Southern China. **Figure S3:** Relationship between the MAOC/SOC ratio and SOC content across seven soil depth layers. A linear regression is fitted for each depth layer, with the annotation reporting the slope and R^2 for each layer. Superscripts denote the significance of each slope against zero (ns, not significant; *$p<0.05$; **$p<0.01$). **Figure S4:** Partial dependency of total soil organic carbon (SOC, a), mineral-associated organic carbon (MAOC, b) and MAOC/SOC ratio (c) on soil clay + silt content. Partial dependence depicts the marginal effect of a variable (i.e., clay + silt) on the response after controlling other variables in the random forest model. **Figure S5:** Environmental predictors and cross-validation statistics of soil carbon stocks. The relative importance of five most important individual predictors for depth-specific total soil organic carbon (SOC, a,c,e) stocks, and mineral-associated organic carbon (MAOC, b,d,f) stocks derived from random forest modeling. RMSE, root mean squared error. R^2, determination coefficients. A description of the abbreviations of the predictors is given in Table S2. **Figure S6:** Uncertainty of predicted soil carbon stocks. Left (a,c,e) and right (b,d,f) panels show uncertainty of soil organic carbon (SOC) and mineral-associated organic carbon (MAOC) stocks in three depth layers, respectively. The uncertainty is estimated as the standard error (SE) of the predictions of 500 trees in the random forest model. NCP, Northeast China Plain; NAS, Northern arid and Semi-arid region; HP, Huang–Huai–Hai Plain; LP, Loess Plateau; QTP, Qinghai–Tibet Plateau; MYP, Middle-lower Yangtze Plain; SB, Sichuan Basin and surrounding regions; YGP, Yunnan–Guizhou Plateau; SC, Southern China. **Figure S7:** Comparison of mineral-associated organic carbon (MAOC) stocks estimated in this study to global mapping products in Chinese croplands. Each grid cell displays the difference between MAOC estimates from global gridded data of Georgiou et al. (2022) and our mapping results (Figure 5) across depth layers. Blue cells denote higher values in the reference databases relative to this study, while red cells indicate lower estimates. **Table S1:** Statistics of farmer survey questionnaires by asking the owner farmers of the sampling field to obtain information about management practices. **Table S2:** Environmental variables and secondary datasets used in this study. The first 78 entries list the environmental variables screened in the predictor analyses; the final eight entries list additional secondary datasets used as mapping inputs or for external comparisons. The definition of climate extremes is adopted from Mistry (2019) and recommended by the World Meteorological Organization. TX, daily maximum near-surface air temperature; TN, daily minimum near-surface air temperature; PR, daily near-surface total precipitation; SPI, standardized precipitation index. *, denotes variables used in the modeling after controlling collinearity. Repository DOIs are provided where an exact data record is available; otherwise, the source publication or official data portal is listed. **Table S3:** Loadings of principal component analysis (PCA) of remote sensing vegetation variables used to derive the vegetation productivity index (VPI). **Table S4:** National stocks of SOC and MAOC in both tons per hectare ($\mathrm{t\,ha^{-1}}$) and gigaton (Pg) at depths of 0–0.3, 0.3–1 and 1–2 m, respectively, in Chinese dryland croplands. The stock at a depth of 0–2 m is calculated as the sum of three soil layers. The total quantities and confidence limits (upper and lower limit of 95% confidence intervals) for SOC and MAOC stocks are calculated by summing the pixel values of the corresponding mappings (Figure 5). The uncertainty of SOC and MAOC stocks is assessed using 100 bootstrap sampling and modeling. **Table S5:** Estimated national stocks of SOC and MAOC in both tons per hectare ($\mathrm{t\,ha^{-1}}$) and gigaton (Pg) at depths of 0–0.3, 0.3–1 and 1–2 m, respectively, across nine agro-ecological zones in Chinese croplands. **Table S6:** Comparison of national SOC density across nine agro-ecological zones in Chinese croplands of present study, SoilGrids, WISE and HWSD (Batjes 2016; FAO et al. 2012; Poggio et al. 2021). **Table S7:** Cropland soil organic carbon (SOC) stock estimates reported by different investigators using legacy soil/inventory data.